nature communications

Article

https://doi.org/10.1038/s41467-025-58146-1

Solid-like condensation of MORF8 inhibits RNA editing under heat stress in Arabidopsis

Received: 23 July 2024

Accepted: 10 March 2025

Published online: 21 March 2025

Check for updates

Jie Wu[1], Yue Wang[2], Haodong Chen[1], Tongda Xu[3], Wenqiang Yang[2] & Xiaofeng Fang[1]

Heat stress inhibits photosynthesis efficiency, thereby suppressing plant growth and crop yield. However, the mechanism underlying this inhibition is not fully understood. Here, we report that the multiple organellar RNA-editing factor 8 (MORF8) forms condensates with solid-like properties in chloroplasts upon heat stress. In vitro data show that the MORF8 condensation is intrinsically heat-dependent and primarily determined by its IDR (intrinsically disordered region). Purification and characterization of MORF8 condensates show that numerous editing factors including PPR proteins and MORFs are partitioned. We provide both genetic and biochemical evidence that MORF8 condensation inhibits chloroplast RNA editing. In agreement, we find that both heat stress and MORF8 condensation lead to reduced editing of RNAs encoding NADH dehydrogenase-like (NDH) complex and impaired NDH activity and photosynthesis efficiency. These findings uncover MORF8 as a putative chloroplastic thermosensor that mediates photosynthesis inhibition by heat and highlight the functional significance of solid material properties of biomolecular condensates.

RNA editing describes processes whereby RNA transcripts undergo nucleotide insertions, deletions, or substitutions[1]. The most prevalent types of base-changing RNA modifications are A-to-I and C-to-U RNA editing. A-to-I RNA editing mediated by Adenosine Deaminase Acting on RNA is dominant in animal species[2]. In plants, C-to-U is the major type of RNA editing, which was first described in plant mitochondria in 1989 and later also in chloroplasts[3–6]. To date, about 500 and 40 editing events have been identified in mitochondria and chloroplast of higher plants, respectively[7]. Abnormal RNA editing can result in defects in plant development and response to abiotic stress[8].

RNA C-to-U editing in plants is postulated to be executed by RNA editosome, comprising of pentatricopeptide repeat (PPR) proteins, multiple organellar RNA editing factors (MORFs), putative deaminase as well as other auxiliary factors[8,9]. Amongst, the PPR proteins recognize specific nucleotide sequences upstream of the target Cs, thereby instructing target recognition[10]. Some PPR proteins contain DYW domains at the C-terminus, which harbor conserved cytidine deaminase (CDA)-like zinc-binding signature residues and therefore are proposed to provide cytidine deaminase activity[11–13]. MORF family proteins function as essential editing factors[14,15]. The family contains nine members, with MORF2 and MORF9 being located in chloroplasts, MORF8 dual-targeted to both chloroplasts and mitochondria and the rest exclusively in mitochondria[15]. Attenuation of MORF function leads to reduced editing efficiency at multiple sites[14,15]. MORF proteins interact with PPR proteins in vivo[16,17]. Structural analysis reveals that MORF binds PPR protein and induces conformational changes that increase the RNA-binding affinity[18,19].

The increasing temperature concomitant with global warming is posing a big challenge to crop yield. High temperature is known to reduce photosynthesis efficiency in chloroplasts, which can occur during chlorophyll biosynthesis, electron transport, photochemical reactions, and CO_2 assimilation[20]. Existing evidence supports that the generation of reactive oxygen species (ROS) by abiotic stress can cause damage to the photosynthetic apparatus, particularly photosystem II

[1]Center for Plant Biology, School of Life Sciences, Tsinghua University, Beijing, China. [2]Key Laboratory of Photobiology, Photosynthesis Research Center, Institute of Botany, Chinese Academy of Sciences, Beijing, China. [3]Haixia Institute of Science and Technology, and College of Life Sciences, Fujian Agriculture and Forestry University, Fuzhou, Fujian, China. e-mail: xffang@tsinghua.edu.cn

(PSII)[21,22]. However, whether and how elevated temperatures affect photosynthesis via PSI is largely unknown. The NADH dehydrogenase-like (NDH) complex has an important role in mediating PSI cyclic electron transport[23]. Here, we report that MORF8 undergoes heat-dependent phase separation in vivo and in vitro. Through mutational and genetic analyses, we provide evidence that the solid-like condensates of MORF8 inhibit RNA editing at multiple sites in *ndhD* and impair NDH activity, leading to compromised photosynthesis. Our findings reveal the molecular basis underlying heat-induced inhibition of photosynthesis.

Results

MORF8 forms solid-like condensates in chloroplasts under heat stress

In our previous identification of potential phase-separated proteins[24], a number of MORF family proteins were highly enriched (Supplementary Fig. 1a, b). We chose the chloroplast-localized MORF8 for condensation analysis in plant cells. To avoid overexpression-induced artificial condensation, we used the native promoter for expression. Consistent with previous report[14], when expressed in tobacco epidermal cells, MORF8 was diffused in the chloroplasts (Fig. 1a). Upon heat stress treatment at 42 °C, MORF8 formed discrete condensates within chloroplasts (Fig. 1a). MORF8 condensation is specific to heat stress, as conditions mimicking hyperosmotic, salt, cold or oxidative stress did not trigger its condensation (Supplementary Fig. 1c). Two other chloroplast-localized MORFs, MORF2 and MORF9, were unable to form condensates upon heat treatment (Supplementary Fig. 1d, e). To further confirm its heat-dependent condensation, we generated a complementation line expressing the full-length genomic sequence of MORF8. The endogenous MORF8 was largely removed by artificial microRNA (amiR-MORF8)-mediated knockdown (Supplementary Fig. 3d). The transgenic copy of *MORF8* was expressed at a comparable level to the endogenous *MORF8* (Supplementary Fig. 2a). In the transgenic plant, MORF8 formed heat-dependent condensates that did not fully dissolve after stress removal for hours (Fig. 1b). The protein level of MORF8 was not altered by heat stress treatment (Supplementary Fig. 2b). We performed fluorescence recovery after photobleaching (FRAP) experiments and found that MORF8 signal within condensates barely recovered after bleaching (Fig. 1c, d). Consistent with this result, MORF8 condensates were not sensitive to 1,6-hexanediol (Fig. 1e), which dissolves liquid-like condensates[25]. We performed a fractionation assay and found that MORF8 was largely reallocated into the insoluble pellet fraction after heat stress treatment (Fig. 1f). These results indicate that heat triggers solid-like condensation of MORF8 in chloroplasts.

Phase separation of MORF8 is intrinsically sensitive to heat

To provide a mechanistic understanding of temperature-dependent condensation of MORF8, we purified recombinant MORF8 that is fused with a green fluorescent protein at the N-terminus. GFP-MORF8 formed condensates in a protein concentration-dependent manner (Fig. 2a). Similar to those observed in vivo, MORF8 condensates in vitro were more solid-like as revealed by the FRAP assay (Fig. 2b, c). All MORF family proteins harbor conserved central MORF box[26] (residues 89–195) and N-terminal uncharacterized region (Supplementary Fig. 1a). Some MORFs including MORF8 contain extended C-terminus that are predicted as intrinsically disordered regions (IDRs) (Supplementary Fig. 1a). The presence of IDRs in MORFs correlated with the enrichment for phase separation potential (Supplementary Fig. 1a, b), suggesting that IDR is important for MORF phase separation. Indeed, deletion of IDR abolished the condensation of MORF8 both in vitro (Fig. 2d, e) and in chloroplasts (Fig. 2f, Supplementary Fig. 2c). MORF box deletion also slightly reduced condensation (Fig. 2e, f). The N domain was mainly responsible for chloroplast localization as MORF8 lacking N domain was localized to cytoplasm and nucleus (Fig. 2f).

In line with heat-dependent condensation in vivo, the number of GFP-MORF8 condensates formed in vitro dramatically increased when the protein sample was incubated at 42 °C for 20 min (Fig. 2g). Quantitative measurement of the turbidity of MORF8 protein solution using ultraviolet-visible spectroscopy confirmed the temperature sensitivity of MORF8 condensation (Fig. 2h, i). To obtain more sensitive measurements, we used dynamic light scattering (DLS) and monitored the apparent hydration radius (Rh) of MORF8 solution during a slow temperature ramp. The particle sizes of MORF8 grew rapidly from 37 °C (Fig. 2j). This was further confirmed by centrifugation-based analysis of condensed fraction (Supplementary Fig. 2d, e). To test if the observed heat-responsiveness of MORF8 in vitro was due to heat-induced aggregation and misfolding, we first used circular dichroism to probe the secondary structural content of MORF8 under different temperatures. The results showed that no obvious alteration of secondary structure occurred with elevating temperature (Supplementary Fig. 2f), suggesting that MORF8 was not denatured in the heat-induced condensates. We further challenged MORF8 condensates formed in vitro with high salt and found that MORF8 condensation was reduced (Supplementary Fig. 2g, h). While treatment with 1,6-hexanediol did not dissolve MORF8 condensates, low concentration of SDS did (Supplementary Fig. 2i). These data support that MORF8 condensates are not heat-induced aggregation. Deletion of IDR completely abolished heat-dependent condensation in vitro while the version lacking the MORF box behaved similarly to wild-type MORF8 (Fig. 2i, j). To address whether IDR alone exhibits heat-dependent condensation, we performed DLS and found that it behaved similarly to full-length MORF8 with elevating temperature (Fig. 2j). Taken together, these results suggest that condensation of MORF8 can directly sense heat.

Condensation of MORF8 inhibits RNA editing in chloroplasts

To date, no loss-of-function mutant for MORF8 has been isolated. We tried to create a knock-out mutant by CRISPR-based gene editing. We were able to obtain heterozygous transformants, but those plants are weak and infertile (Supplementary Fig. 3a, b). No homozygous knockouts were identified, suggesting that complete loss of MORF8 causes lethality. We decided to knock down MORF8 using artificial microRNAs (amiRNAs). Two amiRNAs base-paring with the coding sequence and 3′ untranslated region (UTR), respectively, significantly downregulated *MORF8* mRNA (Supplementary Fig. 3c, d). These plants were small and albinistic (Supplementary Fig. 3e), and exhibited nearly abolished editing at *ndhD*-2 and *psbF*-77 (Supplementary Fig. 3f). We profiled the 34 known C-to-U RNA editing events in *Arabidopsis* chloroplast. Compared to the wild-type, about half of the plastid editing sites showed reduced editing efficiency in the *MORF8* knock-down plants (Fig. 3a), confirming the key role of MORF8 in plastid RNA editing. To further investigate the role of MORF8 in RNA editing, we generated overexpression lines using the CaMV 35S promoter (*35S::MORF8/Col-0*). Unexpectedly, we observed reduced RNA editing efficiency at multiple sites upon MORF8 overexpression compared to Col-0, in particular on genes encoding subunits of the NADH dehydrogenase-like (NDH) complex (Fig. 3b, Supplementary Fig. 3g). In line with this observation, MORF8-overexpressing plants displayed retarded growth and pale green leaves (Fig. 3c), reminiscent of the *MORF8* knock-down phenotypes. This observation is in agreement with the report that a T-DNA insertion mutant caused ectopic *MORF8* expression and exhibited reduced chloroplast RNA editing[14]. We noticed that overexpression of MORF8 led to constitutive condensates without heat stress treatment, which was diminished by IDR deletion (Fig. 3d). These constitutive condensates were also solid-like because full-length but not ΔIDR version of MORF8 was enriched in the pellet fraction in a sedimentation assay (Fig. 3e). The phenotypes caused by MORF8 overexpression can be

https://doi.org/10.1038/s41467-025-58146-1

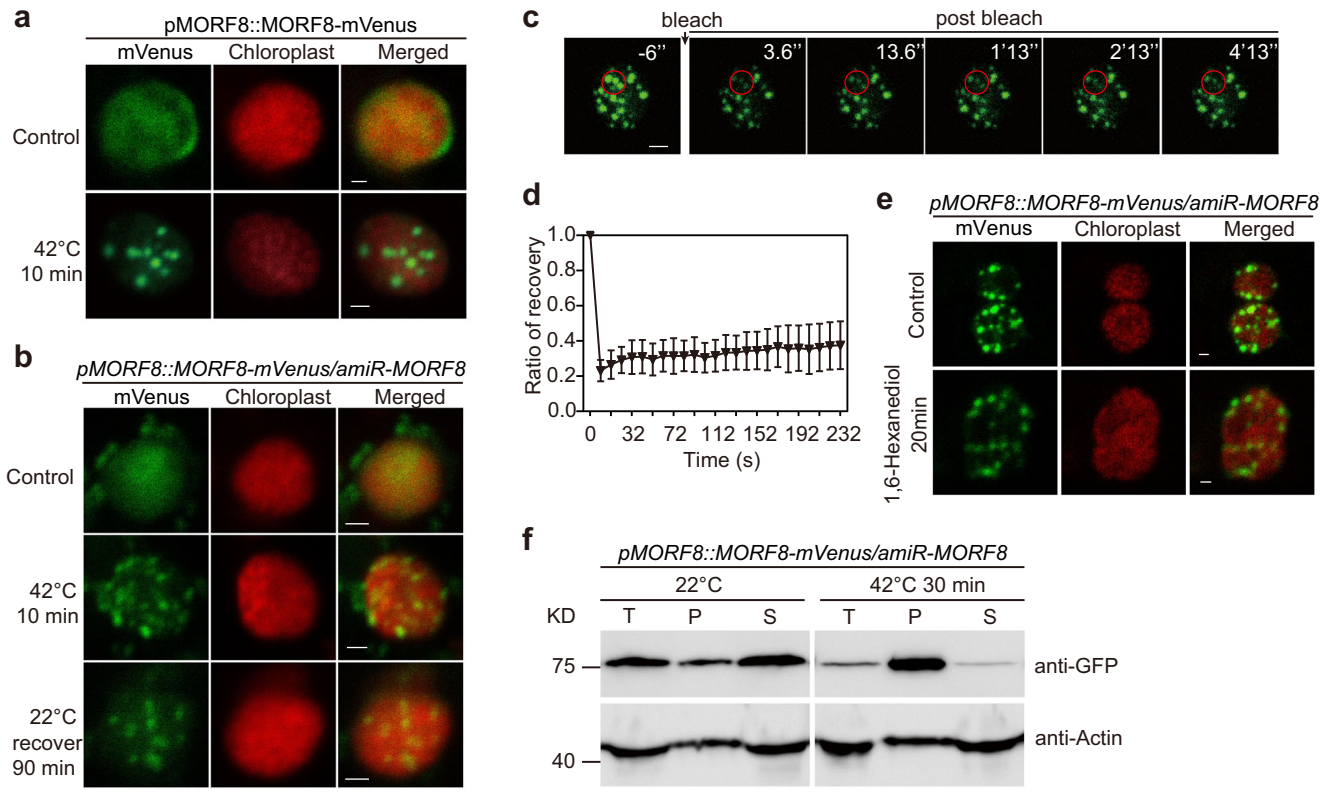

Fig. 1 | MORF8 forms solid-like condensates in response to heat stress. **a** Representative confocal microscopic images of tobacco epidermal cells expressing MORF8-mVenus. The leaf discs were treated at 42 °C for 10 min. Scale bars, 1 μm. **b**, **e** Confocal microscopy of Arabidopsis leaves cells that are treated as indicated. Scale bars, 1 μm. Each experiment was repeated independently for three times with similar results. **c** FRAP of MORF8 condensates formed in Arabidopsis chloroplasts. Red circle indicates the condensates bleached. Time 3.6 s indicates the time of the photobleaching pulse. Scale bar, 1 μm. **d** Plot showing the time course of the recovery after photobleaching. Data are presented as the mean ± SD ($n = 10$). **f** The abundance of MORF8 protein in different fractions of the sedimentation assay. T toal, P pellet, S supernatant. Source data are provided as a Source Data file.

largely attributed to MORF8 condensation because overexpression of MORF8$^{\Delta IDR}$ had no obvious impact on RNA editing as well as plant development (Fig. 3b, c).

To explore other effects of MORF8 condensation, we further examined the splicing of chloroplast genes containing the group II introns via RT-PCR[27]. The results showed that the splicing of 5 genes, including *ndhA*, *rps12*, *trnG*, *trnL*and *petB* was altered in *35S::MORF8/Col-0* but not in *35S::MORF8$^{\Delta IDR}$/Col-0* compared to wild-type Col-0 (Supplementary Fig. 3h). Consistent with this, we observed that a P-class PPR protein CRR16, which was responsible for the efficient splicing of *ndhA* transcript[28], could be recruited into MORF8 condensates (Supplementary Fig. 4d, e). Together, these results suggest that MORF8 condensation regulates post-transcriptional RNA processing in chloroplasts.

MORF8 is dual localized in chloroplasts and mitochondria[14]. We confirmed this dual localization using our stable transgenic plant. In the leaf epidermal cells in which chloroplasts are abundant, we found that MORF8 is predominantly localized in chloroplasts (Supplementary Fig. 3i). We then used root tips for imaging to minimize the effect of chloroplasts and found that MORF8 colocalized well with mitochondria that were labeled by MitoTracker Red (Supplementary Fig. 3j). The small size of mitochondria makes it impossible to observe condensates due to the resolution limit of confocal microscopy. Nevertheless, we measured the editing efficiency for a few selected mitochondria transcripts that were influenced in *rip1*[14]. We found that overexpression of full-length MORF8 but not MORF8$^{\Delta IDR}$ reduced the editing efficiency of these transcripts (Supplementary Fig. 3k). These results suggest that MORF8 condensation may also inhibit the editing in mitochondria.

MORF8 condensates partition PPR proteins

To understand how MORF8 condensation inhibits RNA editing in vivo, we sought out to characterize the proteins that associate with MORF8 condensates. Given the solid property, we were able to purify MORF8 condensates by centrifugation in combination with immunoprecipitation (Fig. 4a). The composition of purified condensates was further analyzed by mass spectrometry (Fig. 4a). We fractionated and purified both the MORF8 condensates resulted from overexpression in *35S::MORF8/Col-0* and condensates formed upon treating *pMORF8::-MORF8-mVenus/amiR-MORF8* plants at 42 °C for 30 min (Supplementary Fig. 4a, b). Proteomic analysis of both condensates gave rise to 241 and 242 proteins, respectively (Fig. 4b). Notably, 110 proteins were shared between the condensates formed by overexpression and heat treatment. Gene Ontology (GO) analysis of the 110 proteins revealed terms such as response to temperature, RNA modification, chloroplast organization (Fig. 4c, d). Among the identified proteins (Supplementary Data 1), PPR proteins were overrepresented (Fig. 4b, Supplementary Data 2). We selected 4 PPR proteins that were highly enriched and tested their colocalization with MORF8. We performed co-expression experiments in Arabidopsis mesophyll protoplasts, in which MORF8 was overexpressed and formed constitutive condensates in an IDR-dependent manner (Supplementary Fig. 4c), and found that all tested PPRs colocalized with MORF8 condensates (Fig. 4e). We also tested a few other PPR proteins, which despite were not robustly enriched in our proteomic analysis but are reported to have interaction with MORF8 and involved in the editing of MORF8-dependent RNAs according to literatures, for colocalization with MORF8 condensates. The results showed that while these PPR proteins alone did not form condensates, they were recruited into MORF8

https://doi.org/10.1038/s41467-025-58146-1

condensates upon co-expression with MORF8 (Supplementary Fig. 4d, e). To test if heat-induced MORF8 condensates also partition PPR proteins, we used a native promoter to drive MORF8 expression in the protoplast to avoid constitutive condensation and exposed the protoplast to a heat stress treatment. The results showed MORF8 formed condensates after heat treatment (Fig. 4f) and the PPR protein CRR21 was recruited into MORF8 condensates (Fig. 4g). We conclude that MORF8 condensates recruit PPR proteins.

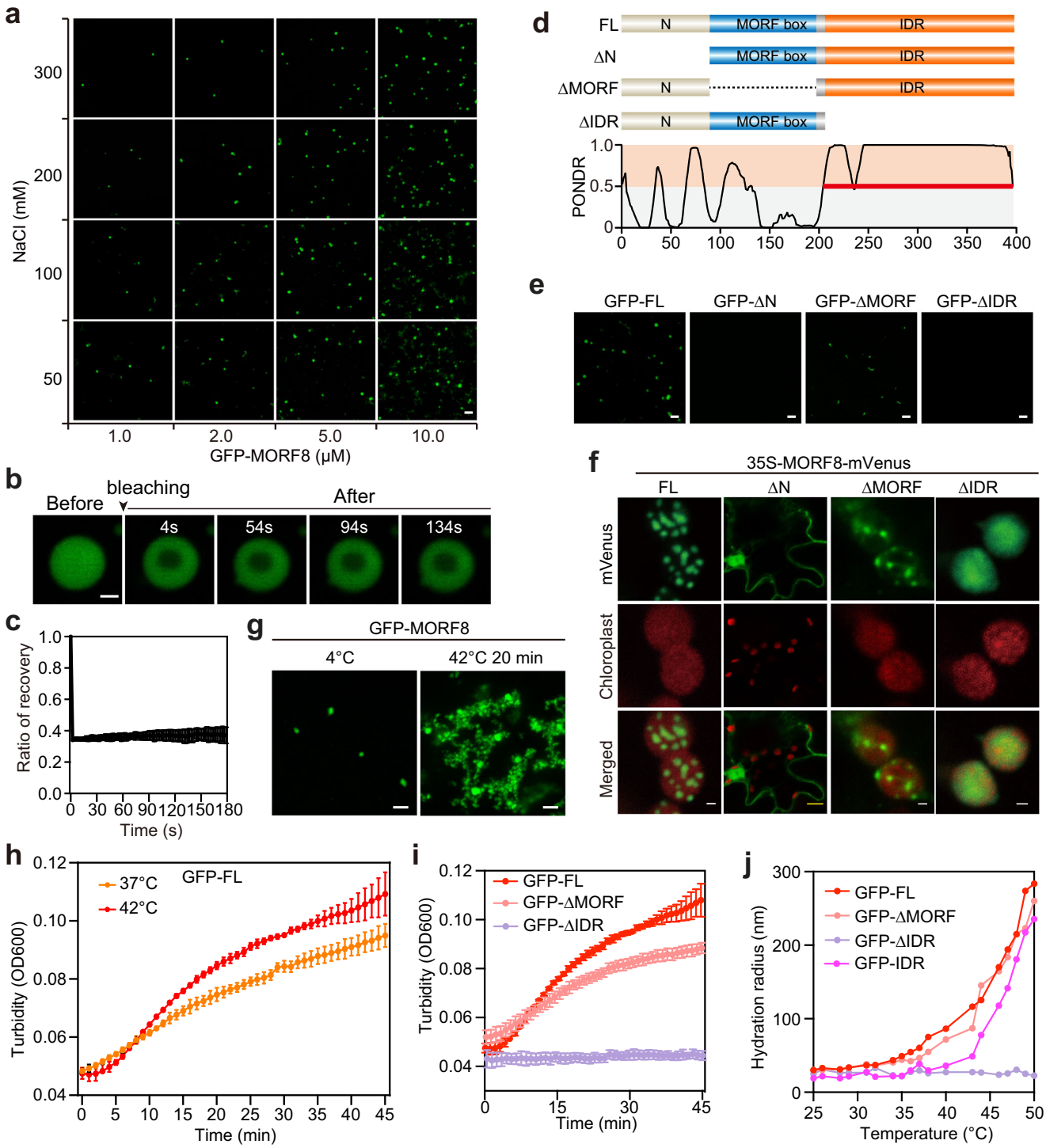

Fig. 2 | MORF8 undergoes heat-dependent condensation in vitro. a Confocal microscopy images of GFP-MORF8 condensates formed at indicated protein and salt concentrations. Scale bar, 10 μm. **b** FRAP of GFP-MORF8 condensate. Time 0 s indicates the time of the photobleaching pulse. Scale bar, 2 μm. **c** Plot showing the recovery after photobleaching of GFP-MORF8 condensates. Data are presented as the mean ± SD ($n = 10$). **d** Top, the domain structures of full-length and variants of MORF8. Bottom, prediction of the disordered regions by PONDR. **e** In vitro phase separation assay of 5 μM indicated proteins. Scale bars, 10 μm. **f** Representative confocal microscopic images of tobacco epidermal cells expressing indicated proteins. Scale bars, white, 1 μm; yellow, 10 μm. **g** In vitro phase separation assay of 5 μM GFP-MORF8 at 42 °C. Scale bars, 10 μm. **h** Turbidity of 5 μM GFP-MORF8 at indicated temperatures. Data are presented as the mean ± SD ($n = 3$). **i** Turbidity of 5 μM indicated proteins at 42 °C. Data are presented as the mean ± SD ($n = 3$). **j** DLS temperature ramp experiments of 1 μM indicated proteins. Source data are provided as a Source Data file.

https://doi.org/10.1038/s41467-025-58146-1

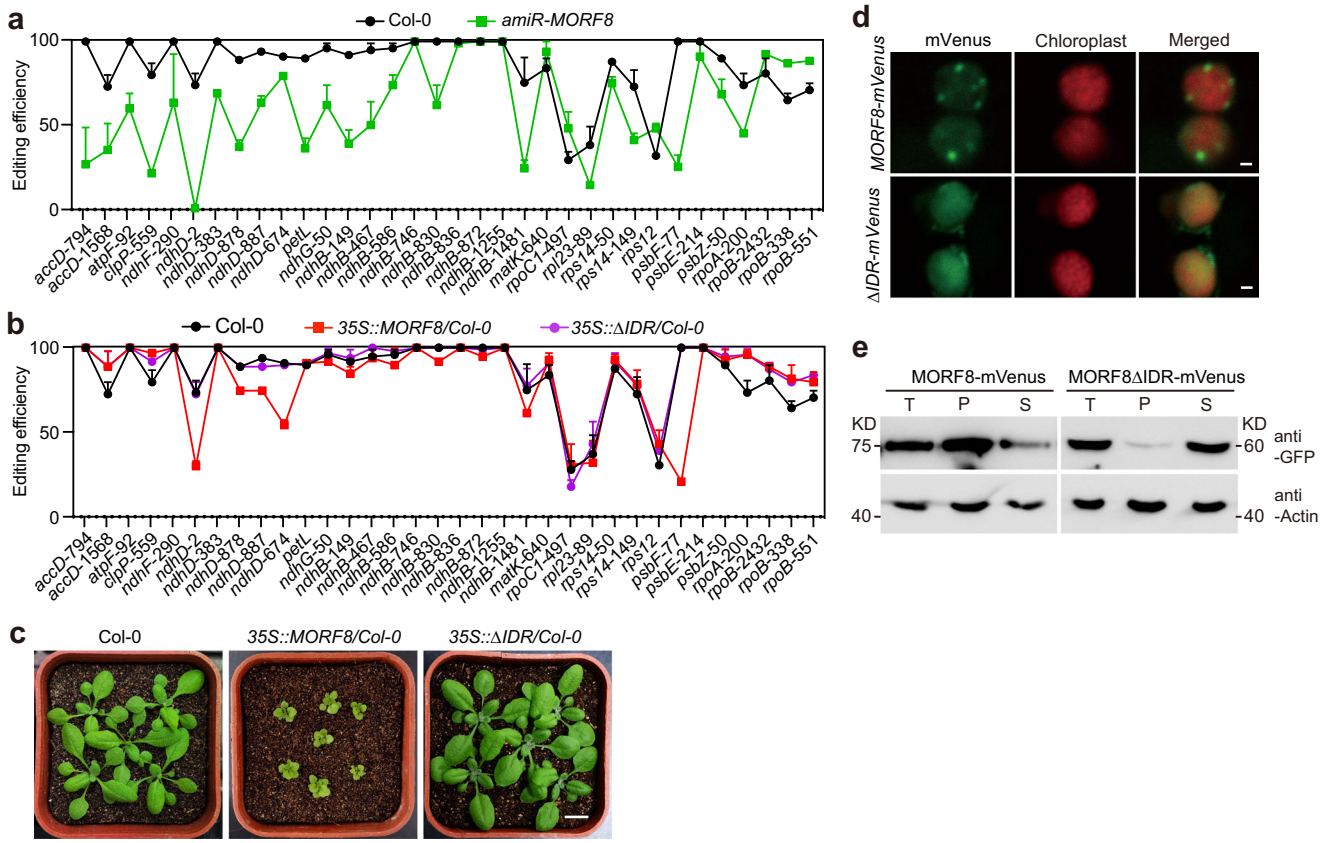

Fig. 3 | MORF8 condensation represses RNA editing in vivo. a Plot of the editing efficiencies of 34 plastid RNA-editing sites in 3-week-old Col-0 seedlings and 10-day-old *amiR-MORF8* knock-down seedlings. Data are presented as the mean ± SD ($n = 3$). **b** Plot of the editing efficiencies of 34 plastid RNA-editing sites in 3-week-old Col-0, *35S::MORF8/Col-0* and *35S::ΔIDR/Col-0* plants. Data are presented as the mean ± SD ($n = 3$). **c** Photographs of 3-week-old Col-0, *35S::MORF8/Col-0* and *35S::ΔIDR/Col-0* plants. Scale bar, 1 cm. **d** Representative confocal microscopic images of Arabidopsis leaf cells expressing full-length or ΔIDR version of MORF8 under 35S promoter. Scale bars, 1 μm. **e** The abundance of MORF8 and MORF8$^{\Delta IDR}$ proteins in different fractions of the sedimentation assay. T toal, P pellet, S supernatant. Source data are provided as a Source Data file.

In addition, most of the MORF family proteins were identified in MORF8 condensate proteomics (Fig. 4b). In agreement, we found that MORF2 or MORF9 did not form condensates but was recruited into MORF8 condensates in vitro (Supplementary Fig. 4f) and in protoplast (Supplementary Fig. 4g, h). This is consistent with the previous report that the absence of MORF8 influences editing at sites targeted by MORF2 and/or MORF9[14,29]. Collectively, these results demonstrate that MORF8 condensation negatively regulates editing by recruiting editing components.

MORF8 condensation inhibits target RNA binding by PPR protein

The MORF box from MORF9 was shown to increase the RNA-binding activity of a PLS-type PPR protein LPA66 in vitro by inducing conformational changes[18]. Given the conservation of the MORF box within the MORF family proteins, we employed in vitro reconstitution to more directly assess the role of MORF8 condensation in regulating the RNA affinity of PPR protein. We initially assessed the RNA-binding capability of LPA66, a PPR protein that is required for editing chloroplast *psbF* transcripts. While LPA66 itself was diffused, it can be recruited into MORF8 condensates in vitro (Supplementary Fig. 5d) and in chloroplasts (Fig. 4e). The binding of LPA66 to *psbF* RNA was significantly enhanced when diffused MORF8 (fused with the solubilizing tag MBP) was present (Supplementary Fig. 5e). We then removed MBP tag to induce MORF8 condensation and found that MORF8 condensates partitioned *psbF* RNA (Supplementary Fig. 5f). Strikingly, addition of LPA66 protein dramatically reduced the amount of *psbF* RNA partitioned by MORF8 condensates (Supplementary Fig. 5f, g), suggesting that LPA66 binds target RNA predominantly in the dilute phase outside MORF8 condensates. We performed a sedimentation assay to separate the RNA-protein complexes in the condensed phase from the dilute phase. Indeed, the electrophoretic mobility shift assay (EMSA) showed that the LPA66-*psbF* RNA complex primarily existed in the supernatant fraction (dilute phase) (Supplementary Fig. 5e). These results indicate that MORF8 is inactivated in the condensed phase. We noticed that the editing efficiency of *psbF-77* was affected by MORF8 overexpression but not by heat stress, both of which induced MORF8 condensation. Consistently, LPA66 was only significantly enriched in the composition of MORF8 condensates resulting from overexpression but not condensates induced by heat (Fig. 4b, c, Supplementary Data 1). These observations suggest the composition of MORF8 condensates dynamically changes depending on external stimuli.

Our data indicate that the constitutive condensation of MORF8 led to dramatic decrease of *ndhD-2* editing efficiency (Supplementary Fig. 3g). DELAYED GREENING1 (DG1) is a PPR protein responsible for the editing of RNAs including *ndhD*, *accD*, and *petL*. It interacts directly with MORF2 and binds target RNAs[30]. Yeast two-hybrid assay showed that MORF8 interacted with DG1 (Fig. 5a). In line with this, while DG1 itself was diffused, it can be recruited into MORF8 condensates in vitro (Fig. 5b) and in chloroplasts (Supplementary Fig. 5a). EMSA and sedimentation analysis of MORF8 with DG1 and *ndhD* showed similar results with LPA66 (Fig. 5c–e). To test whether *ndhD* RNA was co-condensed with MORF8 condensates in vivo, we fractionated the

https://doi.org/10.1038/s41467-025-58146-1

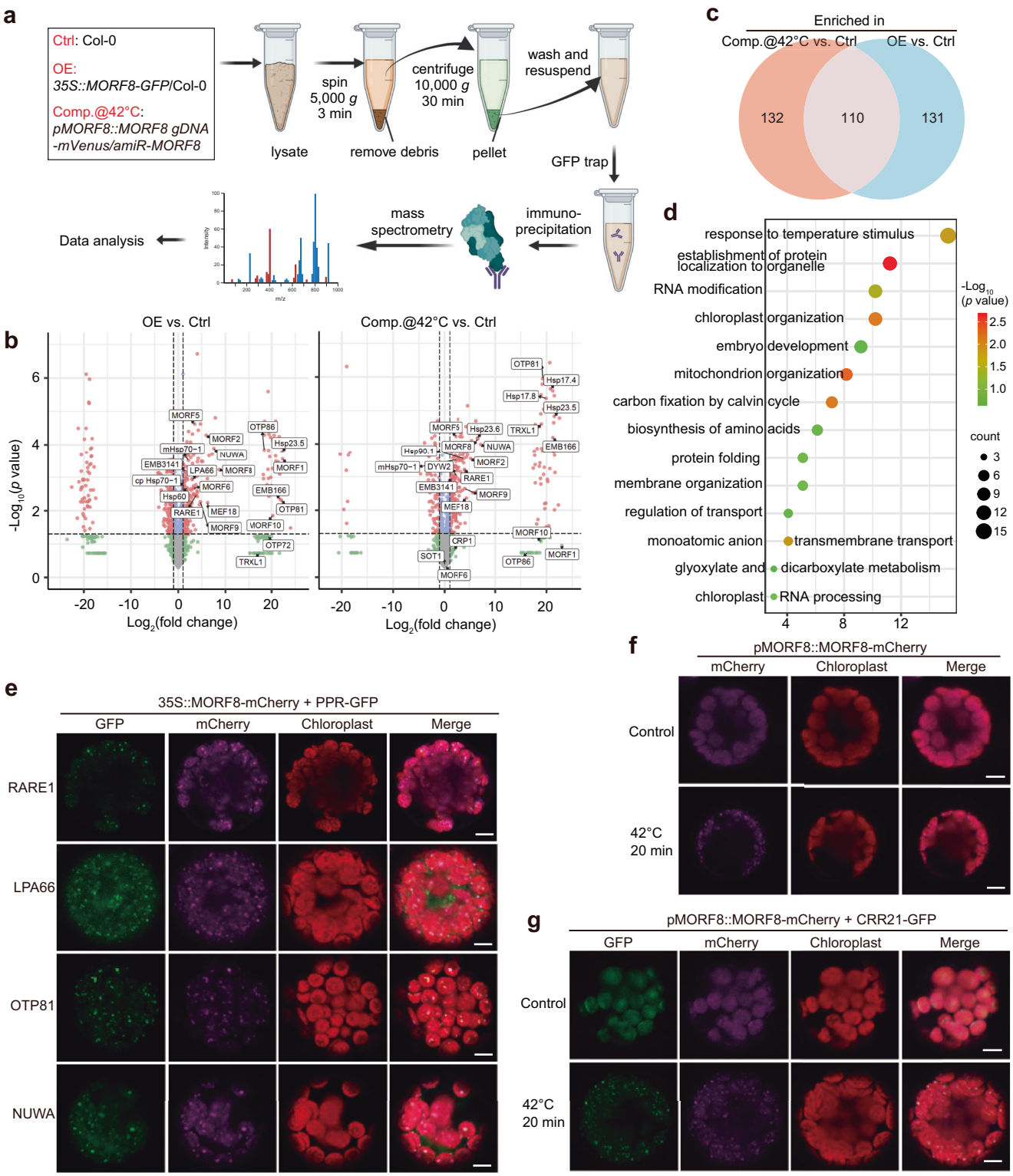

Fig. 4 | PPR proteins were recruited into MORF8 condensates. a Schematic diagram illustrating the purification and characterization of MORF8 condensates. Wild-type Col-0 was used as a background control. Created in BioRender. Fang, X. (2025) https://BioRender.com/j89n207. **b** Volcano plot showing the proteins enriched in MORF8 condensates that were purified from overexpression and heat stress-treated plants, respectively. The *P* values were calculated from three biological replicates. The significance boundaries are based on both Log2 FC > 1 and *P* value of significance <0.05. **c** Venn diagram showing the overlap between two indicated protein sets. **d** Gene Ontology analysis of the 110 overlapped proteins shown in (**c**). The significance boundaries are based on both Log2 FC > 1 and *P* value of significance <0.05. *P* values were calculated using two-tailed *t*-tests. **e** Representative confocal microscopic images of Arabidopsis protoplast cells expressing four PPR proteins enriched in pellet samples with MORF8-mCherry. Scale bars, 5 μm. **f** Representative confocal microscopic images of Arabidopsis protoplast cells expressing full-length genomic DNA of MORF8 driven under its native promoter. Scale bars, 5 μm. **g** Representative confocal microscopic images of Arabidopsis protoplast cells co-expressing CRR21 with MORF8. Cells were treated at 42 °C for 20 min. Scale bars, 5 μm. Source data are provided as a Source Data file.

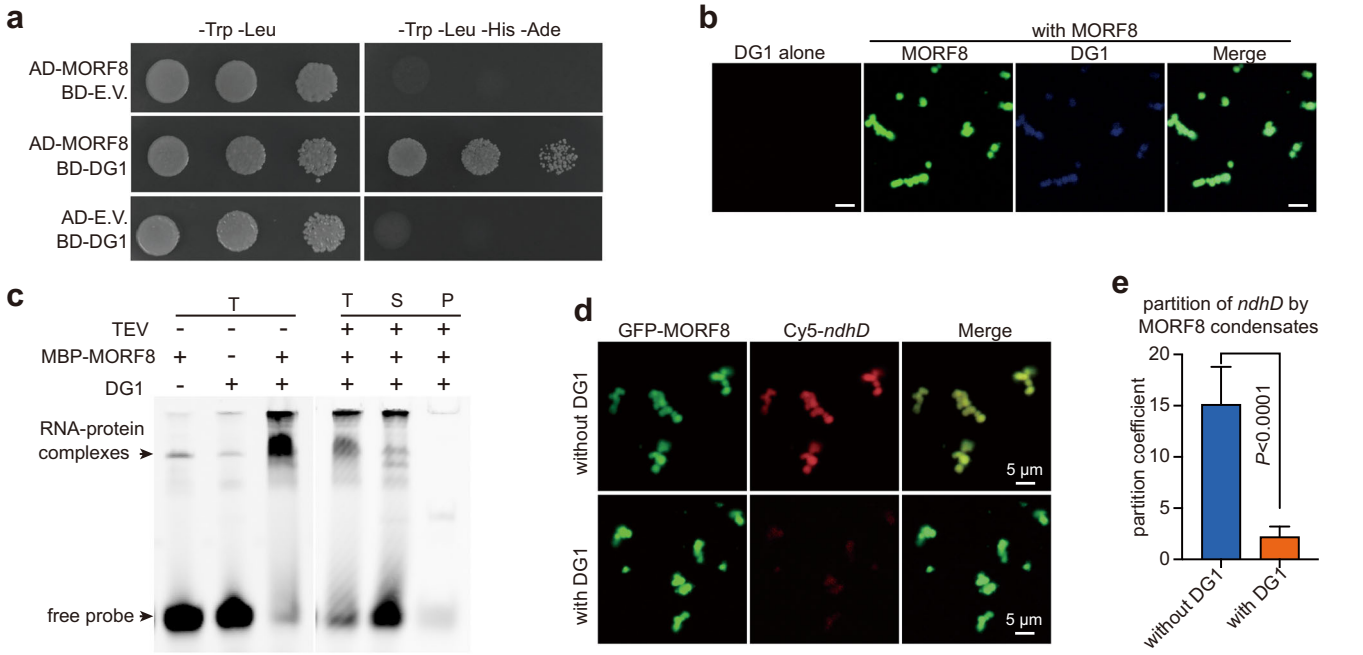

Fig. 5 | MORF8 condensation represses target RNA association with DG1 in vitro. a The interaction between DG1 and MORF8 as determined by yeast two-hybrid (Y2H). E.V., empty vector. **b** Confocal microscopic images showing the partitioning of DG1 (blue) by the MORF8 condensates (green) in vitro. Scale bar, 5 μm. **c** The RNA-binding activity of DG1 with and without MORF8 as determined by EMSA. The final concentrations of MBP-MORF8, MORF8, and DG1 are 5 μM and *ndhD* is 100 nM. T toal, P pellet, S supernatant. **d** Confocal microscopic images showing the partitioning of Cy5-*ndhD* (red) by the MORF8 condensates (green) in the absence or presence of DG1. Scale bars, 5 μm. **e** Quantification of the partitioning efficiency of *ndhD* RNA by MORF8 condensates shown in (**d**). Error bars indicate mean ± SD ($n = 15$), P values were calculated using two-tailed t-tests. Source data are provided as a Source Data file.

extracts from plants treated with or without heat stress (Supplementary Fig. 5h). We reasoned that the amount of target RNAs in soluble phase would decrease if they were condensed into pellet fraction, but we found that heat stress did not reduce the amount of *ndhD* RNA from the soluble phase (Supplementary Fig. 5i). These results indicate that condensation of MORF8 decreases RNA-binding by PPR protein, further supporting that MORF8 condensation inhibits chloroplast RNA editing.

MORF8 condensation and heat lead to impaired NDH activity

The observations that heat induces MORF8 condensation and that MORF8 condensation inhibits chloroplast editing promoted us to investigate whether heat suppresses chloroplast RNA editing. A time course analysis when plants were subjected to heat stress for 1, 3, 6, and 8 h and recovered at normal growth temperature for 1, 3, 6, and 8 h was performed. We observed gradual increase and decrease of MORF8 condensation during and post-heat stress, respectively (Fig. 6a). Analysis of the editing efficiency of *ndhD*-2 showed negative correlation with MORF8 condensation (Fig. 6b). Profiling of all 34 chloroplast editing events upon 8-h heat stress revealed 16 additional sites with reduced editing efficiency (Supplementary Fig. 6a), largely resembling that in *amiR-MORF8* knock-down plants (Fig. 3a). These results indicate that heat-induced MORF8 condensation inhibits RNA editing in vivo.

Most chloroplast editing events result in amino acid changes[31]. However, the functional significance of these editing events is obscure. The *ndhD*-2 site lies within the translation initiation codon of *ndhD* transcript and a defect in *ndhD*-2 editing dramatically impairs the accumulation of the NDH complex and NDH activity[32]. Indeed, we carried out immunoblot analysis of the NdhH subunit and found that conditions reducing *ndhD-2* editing, i.e., heat treatment and overexpression of MORF8, lead to reduction of NDH complex protein level (Fig. 6c, d). The *ndhD* RNA level showed no obvious change (Supplementary Fig. 6b). The NDH complex mediates the cyclic electron transport around photosystem I, which is one of the most important alternative electron transport pathways[33]. To test whether MORF8 condensation modulates NDH activity, we measured the transient increase in chlorophyll fluorescence after turning off actinic light (AL), which reflects NDH-mediated plastoquinone reduction[34]. Compared to Col-0, the transient increase of fluorescence was diminished in *35S::MORF8/Col-0* plants (Fig. 6c, e). In contrast, overexpression of MORF8$^{\Delta IDR}$ had a neglectable impact on it (Fig. 6c, e). This fluorescence increase was also drastically compromised in *amiR-MORF8* plants as well as in heat-stressed plants (Fig. 6c, e). Consistent with this, blue native (BN)-PAGE electrophoresis resolving the composition of photosynthetic protein complexes extracted from the thylakoid membranes[35], revealed lower levels of NDH–PSI complexes in *35S::MORF8/Col-0* and heat-stressed Col-0 plants but not in *35S::MORF8$^{\Delta IDR}$/Col-0* plants (Fig. 6c, f). Finally, the maximum photochemical efficiency of photosystem II Fv/Fm was greatly reduced in MORF8-overexpressing plants but not MORF8$^{\Delta IDR}$-overexpressing plants (Supplementary Fig. 6c).

Together, these results suggest that heat-induced condensation of MORF8 inhibits chloroplast RNA editing, resulting in impaired NDH activity and photosynthesis efficiency.

MORF8 condensation is conserved in crops

Genes encoding MORF proteins are detected in flowering plants but not in other land plants[15,36]. To assess whether the condensation of MORF8 is conserved, we explored the diversity of this protein family in other angiosperms (Supplementary Fig. 7a). Sequence analysis of MORF8 homologs revealed that they all possess long C-terminal IDRs (Supplementary Fig. 7b). We purified MORF8 of rice (OsMORF8) and found that it readily underwent condensation in vitro (Supplementary Fig. 7c). OsMORF8a also exhibited increased turbidity as temperature elevated (Supplementary Fig. 7d). Expression of various truncations of OsMORF8a in tobacco epidermal cells showed that IDR contributed to its condensation (Supplementary Fig. 7e). Furthermore, we expressed two MORF8 homologs from soybean in tobacco and found that they

https://doi.org/10.1038/s41467-025-58146-1

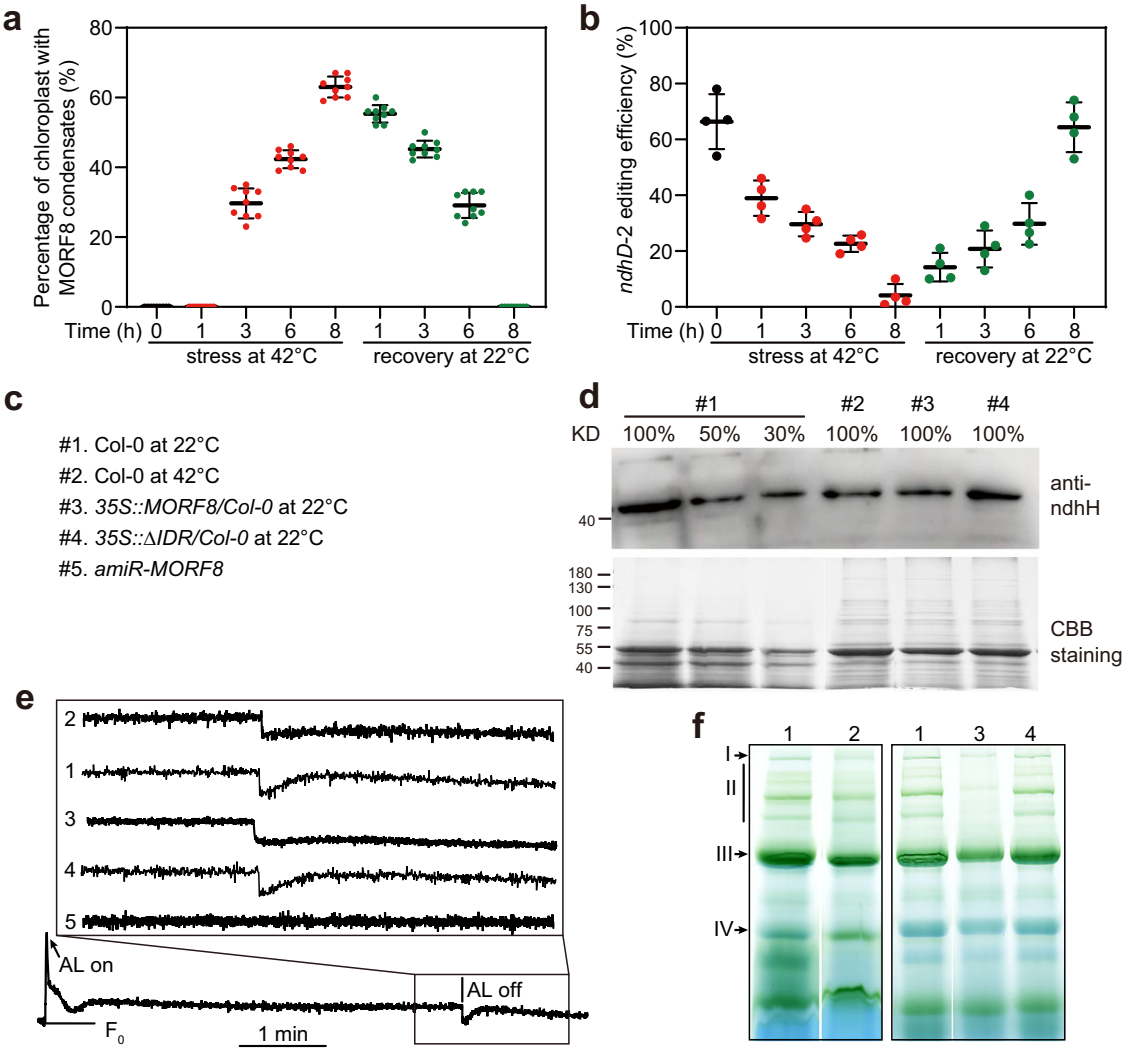

Fig. 6 | MORF8 condensation and heat impair photosynthesis via repressing NDH complex activity. a Quantification of the percentage of chloroplasts containing MORF8 condensates using *pMORF8::MORF8-mVenus/amiR-MORF8* under conditions as indicated. Error bars indicate mean ± SD ($n = 9$). Each replicate contains ~10 chloroplasts. **b** RNA editing efficiency of *ndhD-2* in 3-week-old Col-0 seedling leaves as indicated. Error bars indicate mean ± SD ($n = 4$). **c** Genotypes used in this figure. **d** Immunoblot analysis of NDH complex accumulation using the antibodies against ndhH. Total proteins were isolated from various genotypes as indicated at the top. Aliquots of 10 μg (*Col-0*, 100%), 5 μg (*Col-0*, 50%), 3.25 μg (*Col-0*, 30%), 10 μg (*35S::MORF8/Col-0*), and 10 μg (*35S::ΔIDR/Col-0*) of total protein were loaded. Coomassie Blue (CBB) staining was used as loading control. **e** Analysis of the transient increase in chlorophyll fluorescence after turning off AL in indicated genotypes. The bottom curve indicates a typical trace of chlorophyll fluorescence in the wild-type (WT). Leaves were exposed to AL (50 mmol photons m^{-2} s^{-1}) for 5 min. AL was turned off and the subsequent transient rise in fluorescence ascribed to NDH activity was monitored by chlorophyll fluorimetry. Insets are magnified traces from the boxed area. AL actinic light. **f** BN-PAGE analysis of thylakoid membrane complexes. I, chloroplast NADH dehydrogenase-like (NDH)-PSI supercomplex; II, PSII supercomplexes; III, PSI-LHCI and dimeric PSII; IV, monomeric PSII. Source data are provided as a Source Data file.

also formed condensates in chloroplasts (Supplementary Fig. 7f). We propose that heat-induced MORF8 condensation has a conserved role in regulating RNA editing in flowering plants.

Discussion

Numerous studies have been dedicated to elucidating the impact of heat stress on photosynthetic activity[22]. Here we discover that heat triggers condensation of an RNA editing factor MORF8 in chloroplasts, which under normal growth temperature is soluble and promotes RNA editing by enhancing RNA-binding of PPR protein (Fig. 7). MORF8 condensates exhibit a solid-like state and inhibit RNA binding, compromising the editing of RNAs that include those encoding NDH subunits. Reduced editing impairs NDH activity and photosynthesis efficiency (Fig. 7). In addition, MORF8 condensation is involved in the regulation of RNA splicing in chloroplasts (Supplementary Fig. 3h). Therefore MORF8 condensation finetunes heat response in chloroplasts via regulation of post-transcriptional RNA processing events.

Our data support that MORF8 undergoes solid-like condensation both in vivo and in vitro, suggesting that MORF8 is a putative thermosensor. We show that IDR is mainly responsible for heat sensing and condensation. A recent study reported that a disulfide oxidoreductase TRXz interacts with rice MORFs, and reduces the conserved cysteine disulfide bond within the MORF box, and that oxidized but not reduced MORFs interact with each other[37]. As chloroplasts overproduce ROS under stress conditions[38], it is plausible that MORF8 is oxidized upon heat stress, which enables the homo-dimerization or even homo-oligomerization of MORF8. This together with the contribution from IDR triggers MORF8 condensation under heat stress in chloroplasts. In agreement with this possibility, MORF box deletion also compromised MORF8 condensation both in vivo and in vitro (Fig. 2e, f). Intriguingly, knockout of rice TRXz leads to reduced RNA

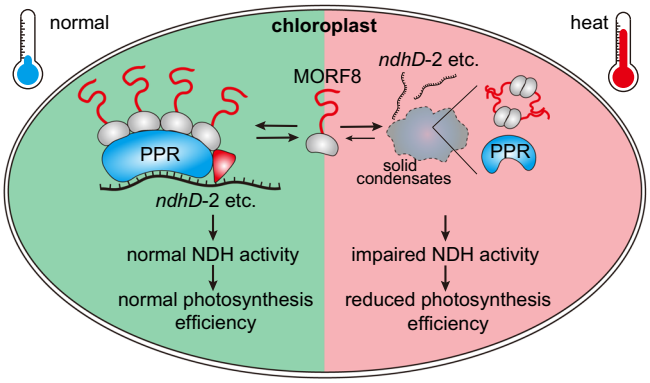

Fig. 7 | A working model for MORF8 condensation in RNA editing regulation under heat stress. RNA editosome component MORF8 is involved in RNA editing under normal growth temperature. Upon heat stress, MORF8 forms solid-like condensates that inhibit target RNA binding by PPR proteins. This reduces the editing of RNAs including those encoding NDH subunits, thereby compromising NDH activity and photosynthesis efficiency.

editing and albino growth phenotype[37]. It is tempting to hypothesize that these phenotypes are largely attributed to MORF8 condensation in the absence of TRXz. Therefore, MORF8 condensation may sense heat stress by both IDR-mediated direct response to temperature and MORF box-mediated reaction to ROS.

Our data confirm that MORF8 plays a crucial role in chloroplast RNA editing, as editing efficiency of 23 sites was decreased in *MORF8* knockdown plants (Fig. 3a). However, only a small subset of these editing sites showed reduced editing efficiency in MORF8-overexpressing plants (Fig. 3b). One explanation is that condensates of MORF8 selectively recruits thereby inhibiting the editing of specific transcripts, but how this selectivity is determined remains to be investigated. In addition, heat affected more editing events than that of MORF8 condensation (Supplementary Fig. 6a), suggesting that other mechanisms may also regulate plastid RNA editing in response to heat stress.

We noticed that similar to MORF8, mitochondria-localized MORF1 and MORF4 have extended C-terminal IDRs (Supplementary Fig. 1a) and were highly enriched by b-isox (Supplementary Fig. 1b), suggesting that MORF1 and MORF4 have the propensity to undergo condensation. Mitochondria contain more editing sites than chloroplast[7] and transcriptomic analyses in Arabidopsis[39] and grape[40] revealed that mitochondrial RNA editing rates are reduced under heat stress. As proper editing of mitochondrial transcripts is important for plant flower development, male fertility, as well as abiotic stress response[41], it is worthy to test whether MORF1 and MORF4 also regulate mitochondrial RNA editing under stress via condensation.

Methods

Plant materials and growth conditions

Seeds were surface sterilized and sown on standard half-strength Murashige and Skoog (MS) (0.22% [w/v] MS, 1% [w/v] sucrose, 0.4% [w/v] Phytagel, Sigma, P8169) at pH 5.8. Media plates were stratified at 4 °C for 2 days and transferred to a growth chamber under long-day conditions (16 h light at 22 °C and 8 h darkness at 18 °C). Ten-day-old seedlings grown on MS medium were typically transplanted to soil. Unless indicated otherwise, 3-week-old plants grown in soil were used for various experiments.

Heat treatment of plant tissues

For imaging of plant cells, leaves from tobacco or 3-week-old Arabidopsis were soaked in liquid half-strength MS medium and treated at the 42 °C water bath for 10 min.

For the RNA editing efficiency test, 3-week-old Arabidopsis grown under normal conditions were transferred to an illumination incubator under long-day conditions at 42 °C as indicated time.

For sedimentation assay in plants, leaves from 3-week-old Arabidopsis were soaked in liquid half-strength MS medium and treated at the 42 °C water bath for 30 min.

Leaves used for BN-PAGE and chlorophyll fluorescence analysis were taken from 3-week-old Arabidopsis treated at 42 °C for 36 h in an illumination incubator.

DNA constructs

To generate the constructs for in vitro protein expression, coding sequences of MORF8, MORF8$^{\Delta IDR}$, MORF8$^{\Delta N}$, MORF8$^{\Delta box}$, OsMORF8a, MORF2, MORF9, DG1 (AA 208-610)[24] and LPA66 (AA 35-515)[18] were amplified and inserted into a modified pET11 expression vector: a solubility tag, maltose binding protein (MBP), was followed by a tobacco etch virus protease (TEV) cleavage site, His6-tag and a GFP, BFP tag. DG1 (AA 208-610) was cloned into the pET11-6×His-HA vector to generate the HA-DG1 and DG1-BFP vectors. LPA66 (AA 35-515) was cloned into the pET11-6×His-BFP vector to generate the LPA66-BFP vector.

For amiRNA constructs, the 21-nucleotide (nt) artificial microRNA sequences base paring with *MORF8* mRNA were designed using the web miRNA designer WMD3. The amiRNA sequences were then integrated into the *MIR167* backbone via overlapping PCR. The resulting precursor fragments were inserted into the pCambia2300 vector between the *KpnI*/*BamH*I restriction sites.

The constructs for overexpression in tobacco epidermal leaf cells and *Arabidopsis* were cloned by inserting the coding sequences into the *EcoR*I site of pCambia1300-35S-V5-mVenus or pCAMBIA1300-35S-N1-Flag (digested with *KpnI*).

To generate the *pMORF8::MORF8-mVenus* construct for complementation in *Arabidopsis* and expression in tobacco epidermal leaf cells, genomic DNA fragments of full-length MORF8, including the promoter of ~2 kb, were amplified from wild-type Col-0 genomic DNA and cloned into the pCambia1300-N1-mVenus vector (digested with *Hind*III and *Spe*I).

To generate transgenic plants, all constructs were introduced into *Agrobacterium tumefaciens* strain GV3101 and transformed into *Arabidopsis* plants via the standard floral dipping method. Positive transformants were selected on half-strength MS plates containing 35 mg/L hygromycin or 50 mg/L kanamycin.

To generate the constructs for transient expression in Arabidopsis protoplasts, the coding sequences of MORF8, MORF2, MORF9, and all the PPR proteins were amplified and inserted into modified pBI221 vectors which contain a mCherry tag or a GFP tag as indicated.

For yeast two-hybrid constructs, the coding sequences of MORF8 and DG1 (AA 48-799) were amplified and inserted between the *EcoR*I and *BamH*I restriction sites of pGADT7 and pGBKT7 using.

All cloning was performed using the ClonExpress II One-Step Cloning Kit (Vazyme, C112). Primers used for vector construction are listed in Supplementary Data 3.

Protein expression and purification

All proteins were expressed in *Escherichia coli* BL21 (DE3) cells (Tiangen) in the presence of 0.6 mM IPTG. Cells were induced overnight at 16 °C, collected, and resuspended in lysis buffer (40 mM Tris, pH 8.0, 500 mM NaCl, 10% glycerol, 1 mM phenylmethylsulfonyl fluoride). The cells were then lysed using an Ultrasonic homogenizer (JY92-IIDN) and centrifuged. The supernatants were first purified with Ni-NTA Sefinose™ Resin (Smart Lifesciences), followed by purification on a Superdex 200 increase 10/300 column (SD200) (GE Healthcare).

In vitro phase separation assay

For in vitro phase separation, MBP tags of MBP-GFP-MORF8, MBP-GFP-MORF8$^{\Delta IDR}$, MBP-GFP-MORF8$^{\Delta box}$, MBP-GFP-MORF8-IDR were released by TEV protease cleavage for 30 min at 4 °C. TEV cleavage efficiency was confirmed by SDS-PAGE analysis. The proteins were diluted into desired concentrations with indicated ionic strengths. The protein samples were incubated at indicated temperatures for the indicated time before imaging. Droplets were visualized in 384 low-binding multi-well 0.17 mm microscopy plates (In Vitro Scientific) using a Zeiss LSM 880 confocal microscope equipped with a 100x/1.60 oil objective.

For the sedimentation assay, 10 μL protein samples were subjected to centrifugation at 14,000 × *g* for 5 min on a micro-centrifuge. The supernatant and pellet were separated into two tubes immediately after centrifugation. The pellet fraction was thoroughly resuspended with the 2 × SDS loading buffer to an equal volume as the supernatant fraction. Proteins from both fractions were analyzed by 8% Tricine-SDS-PAGE followed by Coomassie blue staining. Band intensities were quantified using the ImageJ/Fiji software.

Turbidity measurements

The protein samples were diluted to a final concentration of 5 μM in 40 mM Tris-HCl, pH 8.0, 100 mM NaCl. An aliquot of 100 μL samples were transferred into flat bottom 96-well plates (Corning, 3364) on ice. The turbidity of protein samples was measured at 600 nm using VARIOSKAN FLASH (Thermo) with different temperature settings. Data were collected every minute.

Dynamic light scattering (DLS) measurements

The proteins were diluted to a final concentration of 1 μM in 40 mM Tris-HCl, pH 8.0, 100 mM NaCl. The protein samples of 200 μL were transferred into a quartz cuvette (Wyatt, JC-0247). DLS measurements were performed using DynaPro NanoStar (Wyatt). For data collection, each time point was the average of three 0.25 s acquisitions filtering out samples with a baseline higher than 1.003. The temperature was set to increase at the speed of 1 °C/min. Measurements were recorded every minute. Data was analyzed in the DYNAMICS software with a cumulant fit to the autocorrelation function.

Circular dichroism (CD) spectroscopy

CD measurements were performed on a Chirascan plus (Aimil) using a 1 mm path length cuvette. MORF8 protein was diluted to a final concentration of 0.1 mg/mL (0.9 μM) in HEPES 40 mM Tris-HCl, pH 8.0, 50 Mm NaCl. CD spectra were recorded from 190 nm to 260 nm with a bandwidth of 1 nm, and a 0.5 s integration time with data collected every 1 nm. Each data point was the average of 3 scans. Spectra were baseline corrected using buffer.

RNA electrophoretic mobility shift assay

For RNA EMSA, a 36-nt *ndhD* RNA probe and 23-nt *psbF* RNA probe were synthesized and labeled with Cy5 at the 3′ end. Labeled RNA (100 nM) was incubated with purified DG1-BFP/LPA66-BFP and/or GFP-MORF8 in 30 μL binding buffer (40 mM Tris-HCl, pH 8.0, 1 mM DTT, 100 mM NaCl). After incubation at 4 °C for 30 min, 4 μL loading buffer (1 × TBE, 0.15% Ficoll) was added to the reaction. The resulting protein-substrate complexes were resolved on 6% non-denaturing polyacrylamide gels in 0.5 × TBE buffer (44.6 mM Tris, 44.5 mM boric acid, and 1 mM disodium EDTA). After electrophoresis at 100 V for 60 min, the gels were scanned using Typhoon FLA 9500 (GE Healthcare). The RNA oligo sequence is listed in Supplementary Data 3.

Protein expression in tobacco epidermal cells

Vectors for protein expression and BiFC analysis were transformed into *Agrobacterium tumefaciens* (GV3101). A colony was inoculated into a liquid LB medium and cultured overnight. The cells were collected, resuspended in infiltration buffer (10 mM MES, pH5.6, 10 mM $MgCl_2$, 100 μM acetosyringone), and adjusted to $OD_{600} \approx 0.8$. The resuspended cells were infiltrated into *Nicotiana benthamiana* leaves and waited for 36–48 h before microscopy analyses.

Quantitative RT-PCR

Total RNA was extracted with the Trizol reagent (Invitrogen), treated with DNase I (Promega) to remove DNA contamination, and reversely transcribed by M-MLV (Invitrogen) using oligo(dT) primers. Quantitative PCR was performed on a CFX96 Touch Real-Time PCR Detection System (Bio-Rad) using 2X M5 HiPer SYBR *Premix EsTaq* (Mei5 Biotechnology). *ACTIN* mRNA was detected in parallel and used for data normalization. The primers used for quantitative PCR are listed in Supplementary Data 3.

Analysis of RNA editing

Analysis of RNA editing was performed as described previsouly[30]. In brief, total RNA extracted from leaves of wild-type Col-0 (with or without heat stress treatment), *amiR-MORF8*, *35S::MORF8/Col-0*, and *35S::ΔIDR/Col-0* plants were treated with DNase I and reverse transcribed with random hexamers (Invitrogen). A series of specific primer pairs flanking the editing sites were used for PCR amplification, and the resulting products were subjected to Sanger sequencing. The efficiency of RNA editing was measured by the relative peak heights of the edited nucleotide in ImageJ software. The primer sequences are listed in Supplementary Data 3.

Sedimentation assay in plant extract

Leaves from 3-week-old plants were ground in liquid nitrogen. Half gram fine powder was resuspended in 0.75 mL lysis buffer (20 mM Tris-HCl, pH 7.4, 150 mM NaCl, 4 mM $MgCl_2$, 0.5% NP-40, 5 mM DTT, 1 × protease inhibitor cocktail), incubated at 4 °C for 20 min with rotation. Samples were subjected to brief centrifugation at 5000 × *g* for 3 min. The supernatant was transferred into a new 1.5 mL tube immediately after centrifugation and centrifuged at 10,000 × *g* for 10 min. The pellet fraction was thoroughly resuspended with the 2 × SDS loading buffer. Samples from both pellet and supernatant fractions were analyzed by 8% Tricine-SDS-PAGE.

Total protein preparations and immunoblot analysis

The total proteins were extracted from 3-week-old Arabidopsis leaves, and the protein used for immunoblot analysis of NDH complex was quantified by the LABLEAD bicinchoninic acid kit (B5001). Protein samples were separated by SDS-PAGE gel and transferred to PVDF membranes. Antibodies against GFP (11814460001, Roche), Flag (F1804, Sigma), ndhH (PHY2292S), and Tubulin (Sigma, T5168) were used as primary antibodies. After the primary antibody incubation, horseradish peroxidase (HRP)-conjugated secondary antibodies (GE Healthcare) were used for protein detection by chemiluminescence (Thermo Scientific, 34095).

Thylakoid membrane preparation and BN-PAGE

Isolation of thylakoids was performed as described[37]. Three-week-old leaves were quickly ground at 4 °C in buffer A (10 mM Tricine, pH 8.0, 0.33 M sorbitol, 5 mM EGTA, 5 mM EDTA, and 10 mM $NaHCO_3$). The homogenate was filtered through two layers of Miracloth (Millipore, 475855) and centrifuged at 4200 × *g* for 5 min at 4 °C. The thylakoid pellet was washed twice by resuspending in buffer W (20 mM HEPES, pH 7.6, 5 mM $MgCl_2$, and 2.5 mM EDTA) and centrifugation at 4200 × *g* for 5 min at 4 °C. BN-PAGE was performed as previously described[38]. Briefly, thylakoid samples (equivalent to 1 mg·mL^{-1} chlorophyll) were resuspended in buffer C (25 mM Bis-Tris-HCl, pH 7.0, 20% (w/v) glycerol with 1% (w/v) n-Decyl-β-Maltoside) for 10 min on ice in the dark. The solubilized thylakoids were centrifuged at 15,000 × *g* for 10 min at

4 °C to remove debris, and the supernatant was mixed with 1/10 volume of a sample buffer (100 mM Bis-Tris-HCl, pH 7.0, 0.5 M 6-aminocaproic acid, 30% (w/v) sucrose and 50 mg·mL^{-1} Serva Blue G). Samples containing equal amounts of chlorophyll (15 µg) were resolved on 5–12% gradient gels.

Co-immunoprecipitation

Approximately 8 g of *N. benthamiana* leaves co-expressing MORF8 with other proteins was ground to a fine powder in liquid nitrogen. The powder was lysed with 12 mL lysis buffer (20 mM Tris-HCl, pH 7.4, 150 mM NaCl, 4 mM $MgCl_2$, 0.5% NP-40, 5 mM DTT, 1 × protease inhibitor cocktail) at 4 °C for 30 min. After filtration through Miracloth (Millipore, 475855-1RCN) and brief centrifugation, the supernatant was incubated with 80 µL of GFP-Nanoab-Magnetic Beads (LABLEAD, GNM-25-1000) for 90 min at 4 °C. The beads were washed four times with wash buffer (20 mM Tris-HCl, pH 7.4, 150 mM NaCl, 4 mM $MgCl_2$, 5 mM DTT, 1 × protease inhibitor cocktail) and boiled in 5 × SDS loading buffer. The immunoprecipitates were subjected to western blot analyses.

Mass spectrometry and data analysis

Mass spectrometry was performed as described previously[40]. MORF8 condensates were purified from *35S::MORF8/Col-0* and *pMORF8::MORF8-mVenus/amiR-MORF8* plants that were treated at 42 °C for 30 min by centrifugation in combination with immunoprecipitation. Three biological replicates were performed for this experiment. Protein samples were separated by SDS-PAGE and digested in-gel with trypsin (0.5 ng/µL). The peptides were extracted from gel slices, separated by HPLC, and sprayed into an LTQ Orbitrap Elite System mass spectrometer (Thermo). A database search was performed on the MASCOT server (Matrix Science Ltd) against the IPI (International Protein Index) Arabidopsis protein database. The proteins with peptides > 1 were considered as enriched proteins. A total of 241 and 242 proteins were significantly enriched in *35S::MORF8/Col-0* and *pMORF8::MORF8-mVenus/amiR-MORF8* plants relative to the Col-0 control respectively. The GO annotation was retrieved from the GO Resource (https://geneontology.org/). GO enrichment analysis was plotted by https://www.bioinformatics.com.cn, an online platform for data analysis and visualization. The significance threshold was chosen based on the Benjamini–Hochberg FDR, other parameters are default.

Transient expression in Arabidopsis protoplasts

A. thaliana mesophyll protoplasts were isolated from 4-week-old Col-0 plants as described[39]. Briefly, leaf slices from the middle part of a leaf were incubated in an enzyme solution (20 mM MES, pH 5.7, 1.5% w/v cellulase R10, 0.4% w/v macerozyme R10, 0.4 M mannitol and 20 mM KCl) for 3–4 h. The suspension was centrifuged and washed twice with W5 solution (2 mM MES pH 5.7, 154 mM NaCl, 125 mM $CaCl_2$, and 5 mM KCl). The plasmids were transformed into protoplasts via the PEG-calcium-mediated method (40% PEG3350). The transfected protoplasts were incubated at 22 °C for 16 h in WI solution (0.5 M mannitol, 4 mM MES, pH 5.7, and 20 mM KCl) and imaged by Zeiss LSM880 confocal laser microscope using a 63× NA objective. Data analysis was performed using Fiji/ImageJ.

Chlorophyll fluorescence analysis

NDH activity was monitored by chlorophyll fluorimetry using a Dual PAM portable chlorophyll fluorometer (Waltz). The transient increase in chlorophyll fluorescence after turning off the AL (50 mmol photons m^{-2} s^{-1} for 5 min) was monitored as described[28]. The maximum quantum efficiency of PSII photochemistry ($F_v/F_m = (F_m–F_O)/F_m$) was measured using the IMAGING-PAM M-Series chlorophyll fluorescence system (Heinz Walz GmbH). Three-week-old plants were dark-adapted for 30 min before measurement and were calculated from basic (F_O) and maximum levels of fluorescence (F_m).

Microscopy

For imaging of tobacco epidermal cells and Arabidopsis leaf cells, a small disc from a tobacco or Arabidopsis leaf was soaked in 1/2 MS liquid medium with or without heat, NaCl, mannitol, sorbitol, and other chemicals for the indicated time. The sample was then transferred onto a slide and imaged on a Zeiss LSM880 confocal laser microscope. The excitation/emission settings used were 488/491–535 nm for GFP, 514/517–557 nm for mVenus, and 488/680–720 nm for chlorophyll fluorescence.

For imaging of MORF8 and PPRs in protoplast, mCherry was excited at 561 nm and detected at 579–650 nm.

Fluorescence recovery after photobleaching (FRAP)

In vivo experiment: FRAP of MORF8-mVenus condensates in Arabidopsis was performed on Nikon AX R with NSPARC confocal microscope system using a ×100/1.45 oil objective. Condensates were photobleached using a laser intensity of 30% at 488 nm. Recovery was recorded for every 10 s for a total of 232 s after bleaching.

In vitro experiments: in vitro FRAP experiments were carried out with samples in 384-well microscopy plates using a Zeiss LSM880 confocal laser microscope equipped with 100× oil immersion objective. A small area of droplets was bleached with a 488-nm laser pulse (8 repeats, 100% intensity, dwell time 1 s). Recovery was recorded for every second for a total of 180 s after bleaching.

For all FRAP experiments, recoveries were measured as the fluorescence intensity of the photobleached area normalized to the intensity of the same area before bleaching. Analysis of the recovery curves was carried out with the FIJI/ImageJ.

Statistics and reproducibility

At least three experiments were repeated independently with similar results in Figs. 1a, b, e, f, 2a, e, f, 3d, e, 4e–g and 5b, d and Supplementary Figs. 1c–e, 2c, g, i, 3i, j, 4c–h, 5a, b, d, f and 7c, e, f. At least two experiments were repeated independently with similar results in Figs. 5c and 6d, f and Supplementary Figs. 2b, 3h and 5c, e.

Reporting summary

Further information on research design is available in the Nature Portfolio Reporting Summary linked to this article.

Data availability

The plasmids and experimental data that support the findings of this study are available from the corresponding author upon reasonable request. Proteomics data are provided as Supplementary Data 1. The raw data of proteomics from this study are available at https://doi.org/10.6019/PXD061133. Source data is available for Figs. 1f, 2h, i, 3a, b, e, 5c, e and 6d, f and Supplementary Figs. 2a, b, d, f, h, 3d, h, 4a, b, 5c, d, g, i, 6a, b and 7d in the associated Source Data file. Source data are provided with this paper.

References

1. Gott, J. M. & Emeson, R. B. Functions and mechanisms of RNA editing. *Annu. Rev. Genet.* **34**, 499–531 (2000).
2. Eisenberg, E. & Levanon, E. Y. A-to-I RNA editing—immune protector and transcriptome diversifier. *Nat. Rev. Genet.* **19**, 473–490 (2018).
3. Covello, P. S. & Gray, M. W. RNA editing in plant mitochondria. *Nature* **341**, 662–666 (1989).
4. Gualberto, J. M., Lamattina, L., Bonnard, G., Weil, J. H. & Grienenberger, J. M. RNA editing in wheat mitochondria results in the conservation of protein sequences. *Nature* **341**, 660–662 (1989).

5. Hiesel, R., Wissinger, B., Schuster, W. & Brennicke, A. RNA editing in plant mitochondria. *Science* **246**, 1632–1634 (1989).
6. Hoch, B., Maier, R. M., Appel, K., Igloi, G. L. & Kossel, H. Editing of a chloroplast mRNA by creation of an initiation codon. *Nature* **353**, 178–180 (1991).
7. Takenaka, M., Zehrmann, A., Verbitskiy, D., Hartel, B. & Brennicke, A. RNA editing in plants and its evolution. *Annu. Rev. Genet.* **47**, 335–352 (2013).
8. Yan, J., Zhang, Q. & Yin, P. RNA editing machinery in plant organelles. *Sci. China Life Sci.* **61**, 162–169 (2018).
9. Small, I. D., Schallenberg-Rudinger, M., Takenaka, M., Mireau, H. & Ostersetzer-Biran, O. Plant organellar RNA editing: what 30 years of research has revealed. *Plant J.* **101**, 1040–1056 (2020).
10. Yagi, Y. et al. Pentatricopeptide repeat proteins involved in plant organellar RNA editing. *RNA Biol.* **10**, 1419–1425 (2013).
11. Boussardon, C. et al. Two interacting proteins are necessary for the editing of the NdhD-1 site in Arabidopsis plastids. *Plant Cell* **24**, 3684–3694 (2012).
12. Andres-Colas, N. et al. Multiple PPR protein interactions are involved in the RNA editing system in Arabidopsis mitochondria and plastids. *Proc. Natl. Acad. Sci. USA* **114**, 8883–8888 (2017).
13. Guillaumot, D. et al. Two interacting PPR proteins are major Arabidopsis editing factors in plastid and mitochondria. *Proc. Natl. Acad. Sci. USA* **114**, 8877–8882 (2017).
14. Bentolila, S. et al. RIP1, a member of an Arabidopsis protein family, interacts with the protein RARE1 and broadly affects RNA editing. *Proc. Natl. Acad. Sci. USA* **109**, E1453–E1461 (2012).
15. Takenaka, M. et al. Multiple organellar RNA editing factor (MORF) family proteins are required for RNA editing in mitochondria and plastids of plants. *Proc. Natl. Acad. Sci. USA* **109**, 5104–5109 (2012).
16. Bayer-Csaszar, E. et al. The conserved domain in MORF proteins has distinct affinities to the PPR and E elements in PPR RNA editing factors. *Biochim. Biophys. Acta Gene Regul. Mech.* **1860**, 813–828 (2017).
17. Sandoval, R. et al. Stable native RIP9 complexes associate with C-to-U RNA editing activity, PPRs, RIPs, OZ1, ORRM1 and ISE2. *Plant J.* **99**, 1116–1126 (2019).
18. Yan, J. et al. MORF9 increases the RNA-binding activity of PLS-type pentatricopeptide repeat protein in plastid RNA editing. *Nat. Plants* **3**, 17037 (2017).
19. Royan, S. et al. A synthetic RNA editing factor edits its target site in chloroplasts and bacteria. *Commun. Biol.* **4**, 545 (2021).
20. Hu, S., Ding, Y. & Zhu, C. Sensitivity and responses of chloroplasts to heat stress in plants. *Front. Plant Sci.* **11**, 375 (2020).
21. Takahashi, S. & Murata, N. How do environmental stresses accelerate photoinhibition? *Trends Plant Sci.* **13**, 178–182 (2008).
22. Gururani, M. A., Venkatesh, J. & Tran, L. S. Regulation of photosynthesis during abiotic stress-induced photoinhibition. *Mol. Plant* **8**, 1304–1320 (2015).
23. Yamori, W. & Shikanai, T. Physiological functions of cyclic electron transport around photosystem I in sustaining photosynthesis and plant growth. *Annu. Rev. Plant Biol.* **67**, 81–106 (2016).
24. Zhang, H. et al. Large-scale identification of potential phase separation proteins from plants using a cell-free system. *Mol. Plant* **16**, 310–313 (2023).
25. Kroschwald, S., Maharana, S. & Simon, A. Hexanediol: a chemical probe to investigate the material properties of membrane-less compartments. *Matters* **10**, 201702000010 (2017).
26. Haag, S. et al. Crystal structures of the Arabidopsis thaliana organellar RNA editing factors MORF1 and MORF9. *Nucleic Acids Res.* **45**, 4915–4928 (2017).
27. An, H. et al. ALBINO EMBRYO AND SEEDLING is required for RNA splicing and chloroplast homeostasis in Arabidopsis. *Plant Physiol.* **193**, 483–501 (2023).
28. Yamamoto, H., Sato, N. & Shikanai, T. Critical role of NdhA in the incorporation of the peripheral arm into the membrane-embedded part of the chloroplast NADH dehydrogenase-like complex. *Plant Cell Physiol.* **62**, 1131–1145 (2021).
29. Bentolila, S., Oh, J., Hanson, M. R. & Bukowski, R. Comprehensive high-resolution analysis of the role of an Arabidopsis gene family in RNA editing. *PLoS Genet.* **9**, e1003584 (2013).
30. Sun, J., Tian, Y., Lian, Q. & Liu, J. X. Mutation of DELAYED GREENING1 impairs chloroplast RNA editing at elevated ambient temperature in Arabidopsis. *J. Genet Genom.* **47**, 201–212 (2020).
31. Tseng, C. C., Lee, C. J., Chung, Y. T., Sung, T. Y. & Hsieh, M. H. Differential regulation of Arabidopsis plastid gene expression and RNA editing in non-photosynthetic tissues. *Plant Mol. Biol.* **82**, 375–392 (2013).
32. Kotera, E., Tasaka, M. & Shikanai, T. A pentatricopeptide repeat protein is essential for RNA editing in chloroplasts. *Nature* **433**, 326–330 (2005).
33. Ma, M., Liu, Y., Bai, C. & Yong, J. W. H. The significance of chloroplast NAD(P)H dehydrogenase complex and its dependent cyclic electron transport in photosynthesis. *Front. Plant Sci.* **12**, 661863 (2021).
34. Shikanai, T. et al. Directed disruption of the tobacco ndhB gene impairs cyclic electron flow around photosystem I. *Proc. Natl. Acad. Sci. USA* **95**, 9705–9709 (1998).
35. Kugler, M., Jansch, L., Kruft, V., Schmitz, U. & Braun, H.-P. Analysis of the chloroplast protein complexes by blue-native polyacrylamide gel electrophoresis (BN-PAGE). *Photosynth. Res.* **53**, 35–44 (1997).
36. Takenaka, M. et al. RNA editing in plant mitochondria-connecting RNA target sequences and acting proteins. *Mitochondrion* **19**, 191–197 (2014).
37. Wang, Y. et al. white panicle2 encoding thioredoxin z, regulates plastid RNA editing by interacting with multiple organellar RNA editing factors in rice. *New Phytol.* **229**, 2693–2706 (2021).
38. Li, M. & Kim, C. Chloroplast ROS and stress signaling. *Plant Commun.* **3**, 100264 (2021).
39. Chu, D. & Wei, L. Reduced C-to-U RNA editing rates might play a regulatory role in stress response of Arabidopsis. *J. Plant Physiol.* **244**, 153081 (2020).
40. Zhang, A., Jiang, X., Zhang, F., Wang, T. & Zhang, X. Dynamic response of RNA editing to temperature in grape by RNA deep sequencing. *Funct. Integr. Genom.* **20**, 421–432 (2020).
41. Tang, W. & Luo, C. Molecular and functional diversity of RNA editing in plant mitochondria. *Mol. Biotechnol.* **60**, 935–945 (2018).

Acknowledgements

This work was funded by grants from the National Natural Science Foundation of China (grant nos. 32222015 and 32450060) and the Ministry of Science and Technology of China (grant nos. 2022YFA1303400 and 2024YFA1308100) to X.F.

Author contributions

X.F. conceived, guided, and supervised the project. J.W. performed all the experiments except for BN-PAGE. Y.W. and W.Y. performed BN-PAGE analysis. H.C. and T.X. helped with the CRISPR editing. X.F. and J.W. wrote the manuscript. All authors discussed the results and reviewed the manuscript.

Competing interests

The authors declare no competing interests.

Additional information

Supplementary information The online version contains supplementary material available at https://doi.org/10.1038/s41467-025-58146-1.

Correspondence and requests for materials should be addressed to Xiaofeng Fang.

Peer review information *Nature Communications* thanks the anonymous, reviewer(s) for their contribution to the peer review of this work. A peer review file is available.